Ceramics International 42 (2016) 13855–13862

Contents lists available at ScienceDirect

Ceramics International

journal homepage: www.elsevier.com/locate/ceramint

Enhanced luminescence of a Eu^{3+}-activated double perovskite (Na, Li) $LaMgWO_6$ phosphor based on A site inducing energy transfer

Quan Liu [a,b], Jialin Shen [c], Tian Xu [a,b], Lixi Wang [a,b], Jing Zhang [c], Qitu Zhang [a,b,*], Le Zhang [d,**]

[a] College of Materials Science and Engineering, Nanjing Tech University, Nanjing 210009, China
[b] Jiangsu Collaborative Innovation Center for Advanced Inorganic Function Composites, Nanjing 210009, China
[c] Nanjing Center, China Geological Survey, Nanjing 210016, China
[d] Jiangsu Key Laboratory of Advanced Laser Materials and Devices, School of Physics and Electronic Engineering,Jiangsu Normal University, Xuzhou 221116, China

ARTICLE INFO

Article history:
Received 7 May 2016
Received in revised form
26 May 2016
Accepted 28 May 2016
Available online 30 May 2016

Keywords:
Double perovskite
Phosphors
Structure evolution
White light emitting diodes

ABSTRACT

Li^+ ion substituted $Na_{1-x}Li_xLa_{0.95}Eu_{0.05}MgWO_6$ phosphors were successfully synthesized by an improved sol-gel method using citric acid and polyethylene glycol as complexing agents. The structural evolution was systematically investigated by X-ray diffraction with Rietveld structure refinement and Raman spectra. The layered ordering of A-site cations and a second-order Jahn-Teller distortion of B' cations simultaneously existed in this double perovskite. The decreased symmetry and lattice parameters within the same space group *C2/m* were observed from the Li^+ substituted powders. Upon increasing the Li^+ concentration, the absorption intensities of the $4f-4f$ transitions of Eu^{3+} monotonically increased. Likewise, the intensity of $^5D_0$-$^7F_2$ monotonically increased under the excitations of both near-ultraviolet and blue light, with an enhancement of ten- and six-fold, respectively. The relative intensity ratio of red/orange emissions gradually increased, and the CIE chromaticity coordinates gradually approached those of standard red light. "A site inducing energy transfer" in double perovskite was achieved by selecting a substitution element with a small radius.

1. Introduction

White light emitting diodes (LEDs) have attracted much attention in recent years. A high luminescence efficiency, low power consumption, and environmental friendliness are some of the advantages of white LEDs [1–4]. As known, white light comprises three primary colors. Tricolor phosphors excited by blue LEDs or near-ultraviolet (NUV) LEDs have also been extensively researched [5–7]. However, the luminescence intensity of the red phosphors for the UV LED chip such as $Y_2O_2S:Eu^{3+}$ or $Y_2O_3:Eu^{3+}$ is much lower than those of $ZnS:Cu^+$, Al^{3+} green and $BaMgAl_{10}O_{17}:Eu^{2+}$ blue phosphors, causing the white light to deviate from natural light [8]. Therefore, new red phosphors with efficient absorption, such as tungstate [9,10]/molybdate [11,12], titanate [13,14] and phosphate[15,16], are urgently needed to compensate the red emission and improve the conversion efficiency.

Tungstate and molybdate have recently been widely investigated as excellent hosts because of their broad and strong charge transfer band (CTB) in the NUV-blue band and high quenching concentrations of activator ions. Typically, the double perovskite oxides reported are mainly A_2BMO_6 (A=Ba; B=Ca, Mg; M=W, Mo) [17–19], due to the higher excitation efficiency of CTB from W/Mo-O than from WO_4/MoO_4. As is known, the magnetic dipole transition is permitted and the electric dipole transition is allowed only when the europium ion occupies a site without an inversion center. The slight tilting of BO_6 in A_2BMO_6 has little effect on reducing the symmetry, and the intensity of the electric dipole transition is lower. Then, the emission transition is $^5D_0 \rightarrow {}^7F_1$ (594 nm) rather than $^5D_0 \rightarrow {}^7F_2$ (~615 nm), leading to an emission of the color orange-red rather than pure red. The "$A^+ + A^{3+}$" mode was used to substitute for the "$2A^{2+}$" mode to provide a lower site symmetry for the A-site and thereby change the dominant transition to improve the purity of red [20,21]. As reported, double perovskite $NaLaMgWO_6:Eu^{3+}$ powder has proven to be an excellent phosphor due to its high energy transfer efficiency of CTB and because its luminescence intensity is much higher than that of the red phosphors presently used [22]. However, the excitation

* Corresponding author at: College of Materials Science and Engineering, Nanjing Tech University, Nanjing 210009, China.
** Corresponding author.
E-mail addresses: ngdzqt@163.com (Q. Zhang), njutzl@163.com (L. Zhang).

http://dx.doi.org/10.1016/j.ceramint.2016.05.191
0272-8842/

wavelength in the range of 300–330 nm is far from the emission wavelength of the NUV-LED chip (370–390 nm) or blue chip (~460 nm). Therefore, methods for enhancing the luminescence intensity under the excitation of near-UV light or blue light have attracted much attention.

In a previous work [20], Gd^{3+} (1.11 Å, CN=9) ions with a smaller radius were selected to substitute for La^{3+} (1.36 Å, CN=12) ions based on the "A site inducing energy transfer" in double perovskite, resulting in enhanced luminescence intensity under the excitation of near-UV light and blue light. "A site inducing energy transfer" in double perovskite can result in a luminescence enhancement of Eu^{3+}, which is based on the selection of a substituent element of small radius. As the radius of Li^+ (0.92 Å, CN=8) is smaller than that of Na^+ (1.39 Å, CN=12), it is interesting to consider whether the luminescence properties could be enhanced by using Li^+ to substitute for Na^+. Additionally, a smaller tolerance factor will be achieved if Na^+ is substituted by Li^+ with a smaller radius. The symmetry will then be lower and the parity-forbidden transition is more easily broken, resulting in better color purity. In this paper, based on the above ideas, Li^+ ions were selected to substitute for the Na^+ ions, attempting to enhance the luminescence of this phosphor system. Rietveld structure refinement and Raman spectra were used to confirm the structure's change. An "A site inducing energy transfer" theory was proposed to enhance the luminescence of a (Na, Li)$LaMgWO_6$:Eu^{3+} phosphor under near-UV and blue light. The relationship between the changed environment and the emissions of Eu^{3+} was analyzed in detail to explain its changed emission.

2. Experimental

All powder samples were synthesized by a sol-gel method using citric acid and polyethylene glycol as complexing agents. The starting materials were La_2O_3 (99.99%), Eu_2O_3 (99.99%), Li_2CO_3 (AR), $NaNO_3$ (AR), $Mg(NO_3)_2$ (AR), $(NH_4)_{10}W_{12}O_{41}$ (AR), HNO_3 (AR), $NH_3 \cdot H_2O$ (AR), citric acid (AR) and polyethylene glycol (PEG, Mw between 570 and 630), all of which were directly used without any further purification. The mole ratio of citric acid to the total metallic ions was 3.0:1.0. Stoichiometric rare earth oxides and Li_2CO_3 were dissolved in HNO_3 under vigorous stirring (solution A, S_A), and stoichiometric amounts of all nitrates and the deionized water were added and stirred (solution B, S_B). The ammonium tungstate was dissolved in deionized water (solution C, S_C). The citric acid and PEG were added to the mixed solution of S_A and S_B, and then solution C was gradually added into the mixed solution of all of the metallic ions. The pH value of the solution was then modulated to 6.0–8.0. The temperature in all of the above processes was 60–70 °C, and the mixed solution was then heated to 80–90 °C and continuously stirred until becoming a transparent sol and then a transparent gel. The transparent gel was heated to 180–200 °C to undergo a combustion reaction to become a spumous and fluffy precursor. Finally, the precursor was pre-calcined at 800 °C for 3 h and then calcined at 1100 °C for 6 h. A series of $Na_{1-x}Li_xLa_{0.95}Eu_{0.05}MgWO_6$ (x=0, 0.1, 0.3, 0.5, 0.7, 0.9, 1) powders was prepared.

The crystalline phases were determined by X-ray diffraction (XRD, smartlabTM 9 kW, Rigaku, Japan) using Cu Kα radiation (λ=1.5406 Å) in the range of 5–80° with a step size of 0.02° and scanning rate of 5°/min. Structure refinements were performed using the Rietveld method as implemented in the General Structure Analysis System (GSAS) software. Raman spectra were collected using a Raman spectrometer (Renishaw, RM1000, Britain) with a 514 nm laser beam as the light source. The photoluminescence spectra were measured using a fluorescent spectrophotometer (Lumina, America). The fluorescent decay curves were tested by a fluorescence spectrometer (FLsp920, British) with the detection wavelength 615 nm. All measurements were taken at room temperature.

3. Results and discussion

Fig. 1(a) and (b) show the excitation spectra of the $NaLa_{0.95}Eu_{0.05}MgWO_6$ powders. It could be seen that the excitation spectra of λ_{em}=615 nm and λ_{em}=590 nm have similar shapes, with a strong broad CTB centered at ~320 nm ($O^{2-} \rightarrow W^{6+}$) and the characteristic *f-f* absorption peaks of Eu^{3+} at 395 nm ($^7F_0$-$^5L_6$) and 465 nm ($^7F_0$-$^5D_2$). However, the excitation intensity for λ_{em}=615 nm was far stronger than that for λ_{em}=590 nm. The corresponding emission spectra for ~320 nm, 395 nm and 465 nm are shown in Fig. 1(c). All emission spectra had weak magnetic dipole transitions ($^5D_0$-$^7F_1$, 590 nm) and very strong electric dipole transitions ($^5D_0$-$^7F_2$, 615 nm), indicating that the Eu^{3+} ions were located in a very low crystal symmetry site in this double perovskite $NaLaMgWO_6$ lattice. The only difference was that the CTB excitation had the strongest emission intensity, eight and four times those of λ_{ex}=395 nm and λ_{ex}=465 nm, respectively. Based on this, the phosphors could only be used for NUV chips for white LEDs. Therefore, much work was attempted to enhance the intensity, and a stronger emission close to the practical emission intensity was expected under the excitation of near-UV band or blue light. In this paper, A-site substitution was used to enhance the red luminescence under the excitations of near-UV and blue light.

3.1. Structural evolution of $Na_{1-x}Li_xLa_{0.95}Eu_{0.05}MgWO_6$

The XRD patterns of $Na_{1-x}Li_xLa_{0.95}Eu_{0.05}MgWO_6$ are shown in Fig. 2 and can be readily indexed to the monoclinic double perovskite structure of $NaLaMgWO_6$ (JCPDS #88-1761). The tolerance factors (t, formula 1) of $Na_{1-x}Li_xLa_{0.95}Eu_{0.05}MgWO_6$ are shown in Table 1, which determine the crystal structure of double perovskite [23]. r_A, $r_{A'}$, r_B, $r_{B'}$ and r_O are the radii of A-site, A'-site, B-site, B'-site and oxygen ions, respectively. Upon increasing the concentration of the smaller radius Li^+, the tolerance factor gradually decreases from 0.948 to 0.868. Clearly, the structure of double perovskite exists stably with no impurity phase when $0.868 \leq t \leq 0.948$.

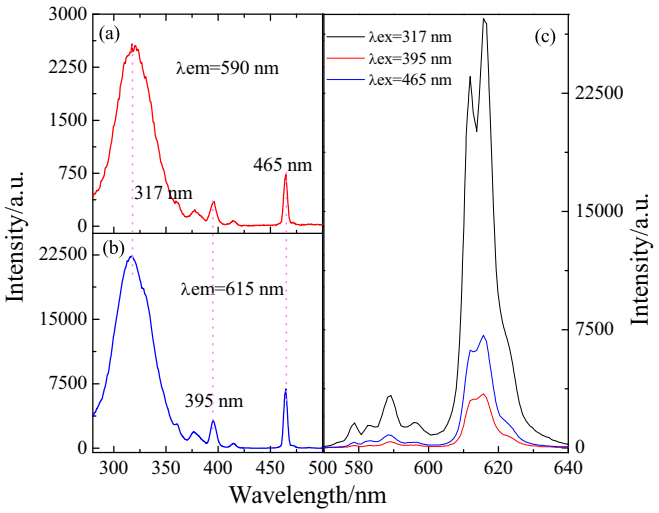

Fig. 1. Excitation spectra (a: λ_{em}=590 nm; b: λ_{em}=615 nm) and (c) emission spectra of $NaLa_{0.95}Eu_{0.05}MgWO_6$ powders.

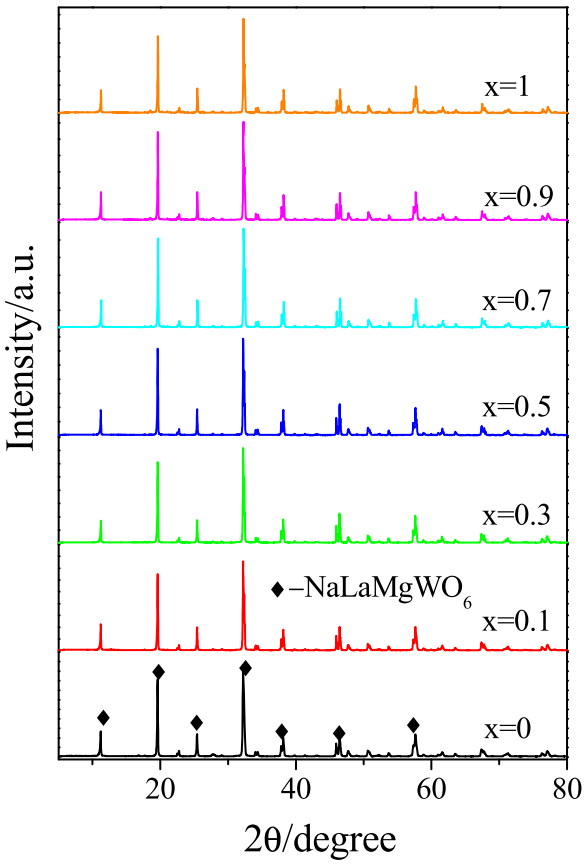

Fig. 2. XRD pattern of $Na_{1-x}Li_xLa_{0.95}Eu_{0.05}MgWO_6$ (x=0, 0.1, 0.3, 0.5, 0.7, 0.9, 1).

Table 1.
Crystallographic data of $Na_{1-x}Li_xLa_{0.95}Eu_{0.05}MgWO_6$.

X values	0	0.1	0.3	0.5	0.7	0.9	1
Tolerance factor	0.948	0.940	0.924	0.908	0.892	0.876	0.868
Space group	*C*2/*m*	*C*2/*m*	*C*2/*m*	*C*2/*m*	*C*2/*m*	*C*2/*m*	*C*2/*m*
a, Å	7.8147	7.8176	7.8120	7.8134	7.8111	7.8079	7.8083
b, Å	7.8211	7.8220	7.8187	7.8175	7.8122	7.8098	7.8105
c, Å	7.8961	7.8939	7.8942	7.8932	7.8910	7.8886	7.8860
V, Å^3	482.705	482.605	482.169	482.114	481.522	481.03	480.941
wRp, %	9.58	9.55	10.38	9.35	10.47	10.08	11.60
Rp, %	6.69	7.19	7.56	6.94	7.77	6.89	8.01

Table 2.
Crystalline and ordered domain sizes for A and B sites with different Li^+ concentrations.

x	CS/nm	ODS-A/nm	ODS-B/nm
0	78.7	72.1	54.3
0.1	82.7	77.3	65.8
0.3	80.5	77.5	71.3
0.5	78.3	77.4	74
0.7	82.5	78.7	67.2
0.9	92.8	81.2	62.8
1	92.9	81.7	60.7

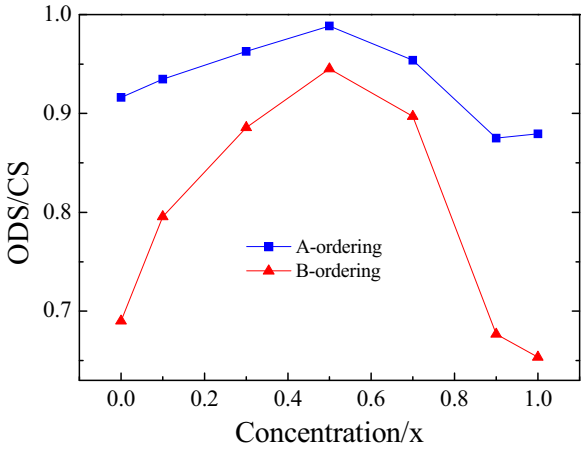

Fig. 4. Ratios of ordered domain size (ODS)/crystalline size (CS) for A and B sites of $Na_{1-x}Li_xLa_{0.95}Eu_{0.05}MgWO_6$ powders (x=0, 0.1, 0.3, 0.5, 0.7, 0.9, 1) with different Li^+ concentrations.

$$t = \frac{r_A + r_{A'} + 2r_O}{\sqrt{2}(r_B + r_{B'} + 2r_O)} \quad (1)$$

In addition, XRD was highly sensitive to the presence of cation ordering, which could be determined by the presence of superlattice reflections. The superlattice diffraction peaks at ~19.0° (0 1 1) and ~38.0° (2 1 1) indicate the long-range ordering of B-site cations (Mg/W) in a rock-salt fashion, and the appearance of a 25.6° (1 1 1) peak demonstrates the layered ordering of A-site cations (Na/Li/La/Eu) [24,25]. The layered ordering of A-site cations creates a bonding instability that is compensated for by a second-order Jahn-Teller (SOJT) distortion of the B' cations [26]. These two distortions are synergistic, and the removal of one leads to the disappearance of the other.

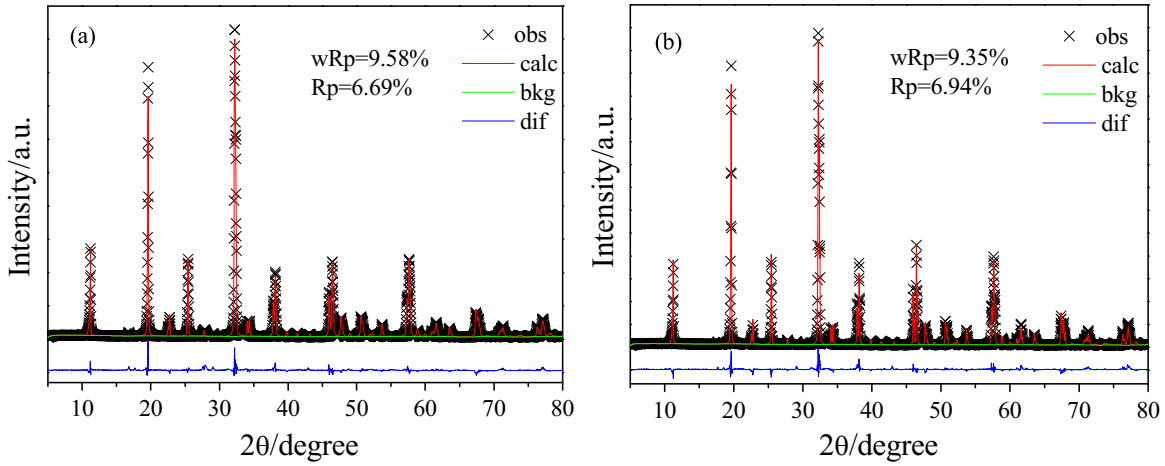

Fig. 3. Rietveld refinement of the observed XRD pattern for (a) $NaLa_{0.95}Eu_{0.05}MgWO_6$ and (b) $Na_{0.5}Li_{0.5}La_{0.95}Eu_{0.05}MgWO_6$.

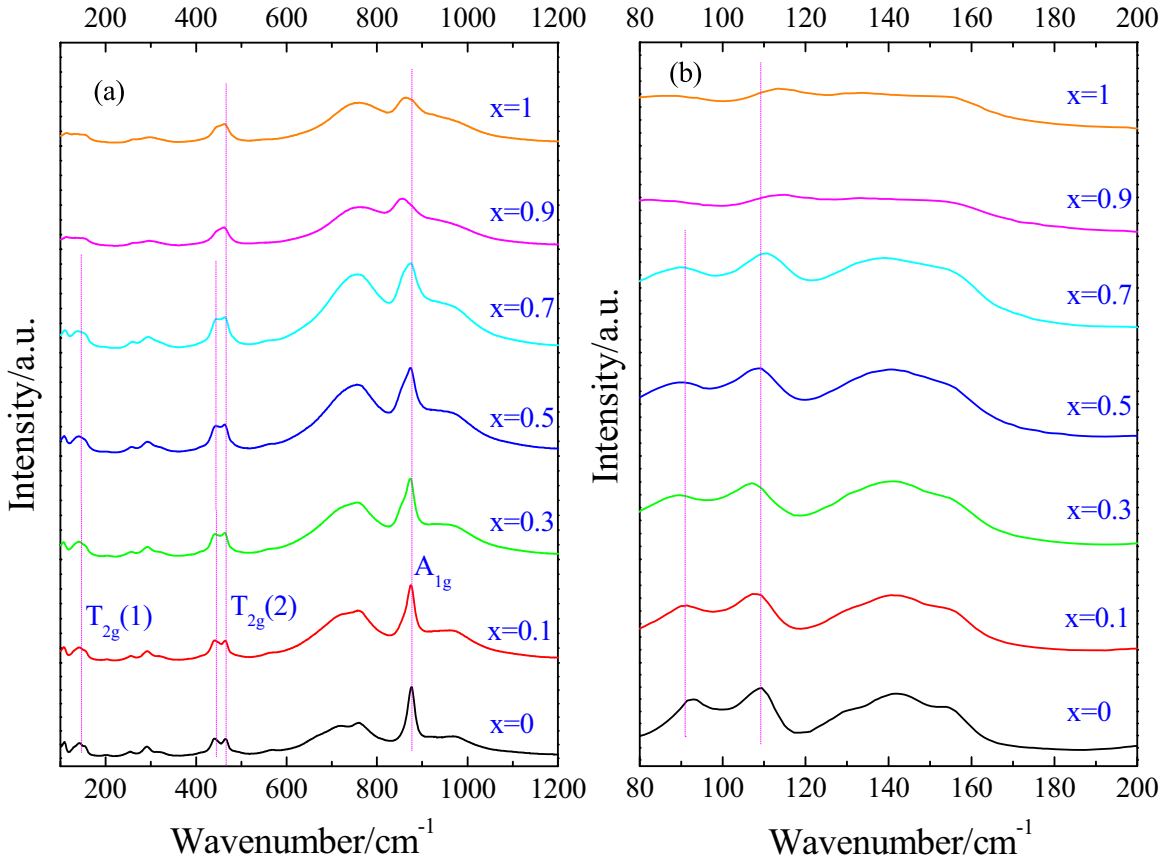

Fig. 5. Raman spectra in the range of (a) 80–1200 cm^{-1} and (b) 80–200 cm^{-1} for $Na_{1-x}Li_xLa_{0.95}Eu_{0.05}MgWO_6$ powders (x=0, 0.1, 0.3, 0.5, 0.7, 0.9, 1) with different Li^+ concentrations.

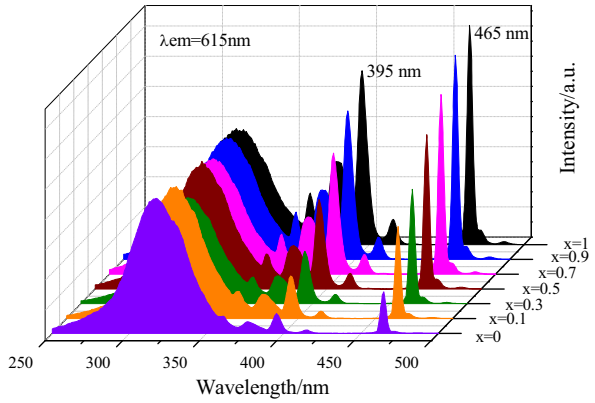

Fig. 6. Excitation (λ_{em}=615 nm) spectra of $Na_{1-x}Li_xLa_{0.95}Eu_{0.05}MgWO_6$ (x=0, 0.1, 0.3, 0.5, 0.7, 0.9, 1).

XRD was only used to perform a preliminary structural characterization of these samples, and Rietveld refinements were carried out to confirm the structures and extract the lattice parameters. Generally, the undistorted and fully ordered AA'BB'O_6 perovskite has tetragonal symmetry and belongs to the space group *P4/nmm*. However, the octahedral tilting would lower its symmetry. The undoped $NaLaMgWO_6$ has degenerated into a monoclinic unit cell, and its two possible space groups are $P2_1$ (Glazer tilt system $a^-a\text{-}c^+$, from JCPDS Card.) and *C2/m* ($a^0b^-c^0$), and their approximate cell dimensions are $\sqrt{2}a_p \times \sqrt{2}a_p \times 2a_p$ and $2a_p \times 2a_p \times 2a_p$ (a_p being the cell edge of the basic ABO_3 cubic perovskite) [24,27], respectively. Therefore, for all samples, the starting models for the refinements of the phases were taken from the double perovskite space groups of $P2_1$ and *C2/m*, respectively. The results showed that the starting model with *C2/m* provides a better fitting for all samples with different doping concentrations of Li^+, even with a complete substitution of Li^+ for Na^+. Typical observed and calculated best fits for the samples are shown in Fig. 3 for x=0 (a) and x=0.5 (b), including the difference in the powder diffraction profiles and the expected Bragg reflections. The refined R-values were 9.58%/9.35% (*wRp*), 6.69%/6.94% (*Rp*) for x=0/0.5, respectively. When x=0, the lattice parameters were 7.8147 × 7.8211 × 7.8961 Å, and the lattice volume was 482.605 Å^3. When x=0.5, the lattice parameters were 7.8134 × 7.8175 × 7.8932 Å, and the lattice volume was 482.114 Å^3. These results suggest that the refinements are in good agreement with the space group in all respects, and the tilting of the BO_6 octahedron weakens the symmetry of double-perovskite. All samples belong to the tilt system $a^0b^-c^0$, where the b^- indicates an out-of-phase tilt around the b-axis, and (Na/Li)$LaMgWO_6$ powders with a *C2/m* space group have a larger lattice volume, which is beneficial to enlarging the distance between neighboring Eu^{3+} ions.

The structural refinements indicate that the degree of cation ordering in these compositions is nearly complete. Generally, if all crystals are assumed to be free of strains and faults, the peak broadening in the X-ray diffraction pattern is due only to the area of the reflecting planes, which is often taken as the crystalline size, according to the Scherrer formula (formula (2)) [20], where *L* is the crystalline size (nm), λ the wavelength of the X-ray source (nm), *FWHM* the full width at half maximum (rad), and θ_0 the diffraction angle (deg). *L* is considered as an average crystal dimension perpendicular to the reflecting planes. Nevertheless, *L* should be considered as the ordered domain's size if *FWHM* is calculated according to the superlattice reflection peaks from the XRD

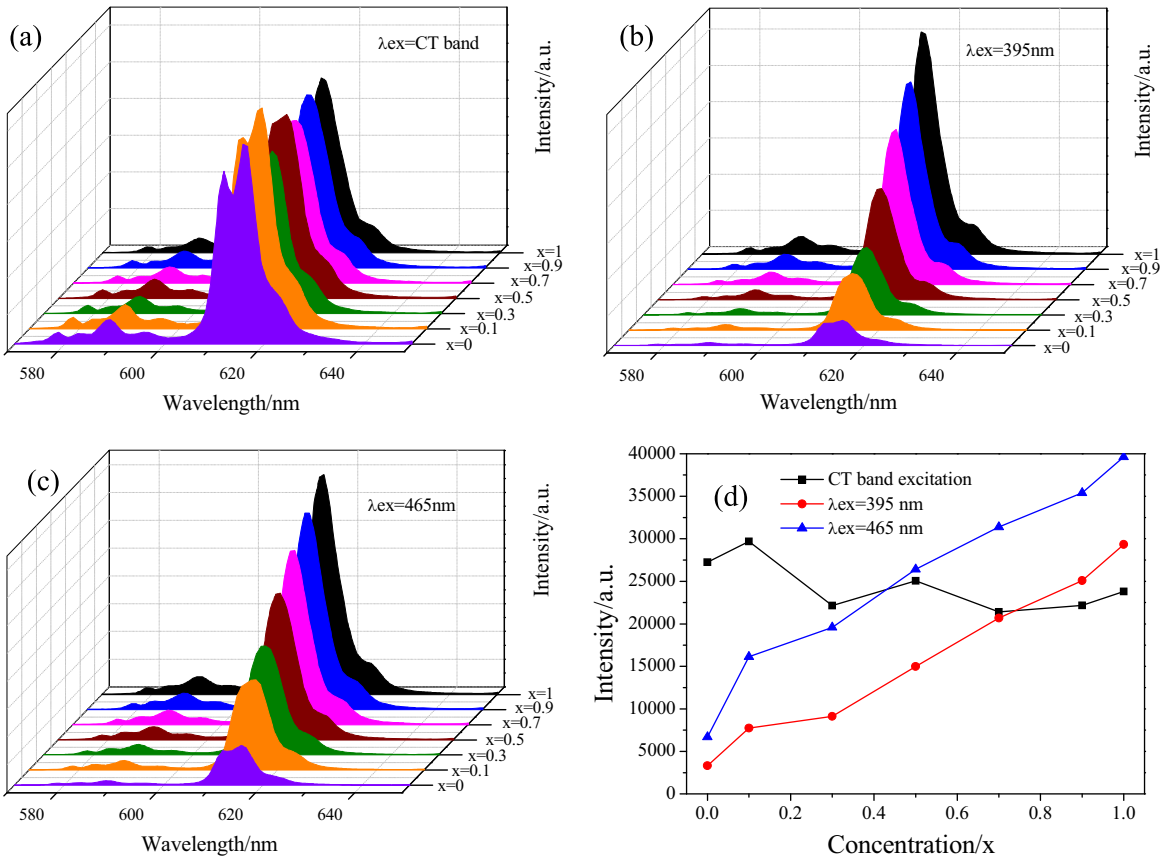

Fig. 7. Emission spectra of $Na_{1-x}Li_xLa_{0.95}Eu_{0.05}MgWO_6$ (x=0, 0.1, 0.3, 0.5, 0.7, 0.9, 1) (a: λ_{ex}=CT band; b: λ_{ex}=395 nm; c: λ_{ex}=465 nm) and (d) the intensity variation of $^5D_0$-$^7F_2$ transition under different excitations.

patterns. Here, the long-range ordering of B-site cations (Mg/W) in rock-salt fashion is observed from the superlattice peaks at ~19° (0 1 1) and ~38° (2 1 1), while the layered ordering of the A-site cations Na/Li/La/Eu is obtained from the diffraction peak at ~25° (1 1 1).

$$L = \frac{0.9\lambda}{FWHM \times \cos\theta_0} \quad (2)$$

Based on the above statements, the ordered domain sizes (ODS) and the crystalline size (CS) for the A and B sites of $Na_{1-x}Li_xLa_{0.95}Eu_{0.05}MgWO_6$ samples were calculated and are listed in Table 2. It can be seen that the ODS-A sites increased monotonically in the range of 72–82 nm, while the ODS-B sites first increased and then decreased in the range of 54–74 nm. This is because the type of ions on the A-site and their amount changes with the gradual substitution of Li^+ for Na^+, and the ordering of the ions on the A-site would vary accordingly, even at the same calcination temperature. The SOJT distortion of the B' cations, compensating for the instability of the A-site cations, led to the variation of the ODS-B sites. The ratios of ODS/CS for the A and B sites of all samples are plotted in Fig. 4. The ODS/CS for the A-site was relatively stable approximately 0.9, while that for the B-site has broader variability. The ODS/CS for both the A-site and B-site first increased and then decreased and reached a maximum value when x=0.5. This is because Na/Li =1:1 is more conductive than the non-equal proportion (e.g., 0.1/0.9 or 0.9/0.1) to obtain a more ordered arrangement. Therefore, doping with Li^+ ions affected the ordered domain sizes for both the A-sites and B-sites.

Fig. 5 shows the Raman spectra of $Na_{1-x}Li_xLa_{0.95}Eu_{0.05}MgWO_6$ powders with different Li^+ concentrations. Both $NaLaMgWO_6$ and A_2CaMoO_6 (A=Sr/Ba) have a double perovskite structure with a rock-salt ordering of B/B' ions, and they may have a great similarity in their Raman spectra. According to Ref. [28], there are four Raman active modes in Ba_2CaMoO_6: $T_{2g}(1)$, $T_{2g}(2)$, Eg and A_{1g}, located at ~105, ~407, ~647 and ~804 cm^{-1}, respectively. For $NaLaMgWO_6$, its Raman spectrum would be more complex than that of Ba_2CaMoO_6 due to its lower symmetry (cubic *Fm3m* for Ba_2CaMoO_6, monoclinic *C2/m* for $NaLaMgWO_6$). The tilting junction of the $(Mg/W)O_6$ octahedra and the layered order of Na/La would result in the splitting of $T_{2g}(1)$ and $T_{2g}(2)$ in the ranges of 100–200 cm^{-1} and 300–500 cm^{-1} into multi-peaks. The $T_{2g}(1)$ mode is an A-site cation related vibration resulting from an A-site cation and coordinated oxygen atoms, and the A_{1g} mode is a fully symmetric breathing vibration of oxygen octahedrons. Furthermore, the A_{1g} mode has a relatively small correlation radius, and its vibration is only confined in the short-range correlation of the atoms, while the $T_{2g}(1)$ mode has a larger correlation radius. Thus, $T_{2g}(1)$ is sensitive to A-site substitution, whereas A_{1g} is sensitive to B-site substitution. With the increasing Li^+ concentration, both the $T_{2g}(1)$ mode and A_{1g} mode significantly weakened. The weakened $T_{2g}(1)$ mode resulted from the A-site doping, while the weakened A_{1g} mode resulted from the SOJT distortion of the B' cations.

3.2. *Photoluminescence of $Na_{1-x}Li_xLa_{0.95}Eu_{0.05}MgWO_6$*

Fig. 6 shows the excitation spectra of $Na_{1-x}Li_xLa_{0.95}Eu_{0.05}MgWO_6$ phosphors with different Li^+ concentrations (λ_{em}=615 nm). The spectra consist of a broad band due to the charge transfer transition from oxygen to tungsten (O^{2-}-W^{6+}, centered at ~320 nm) and some sharp lines due to the

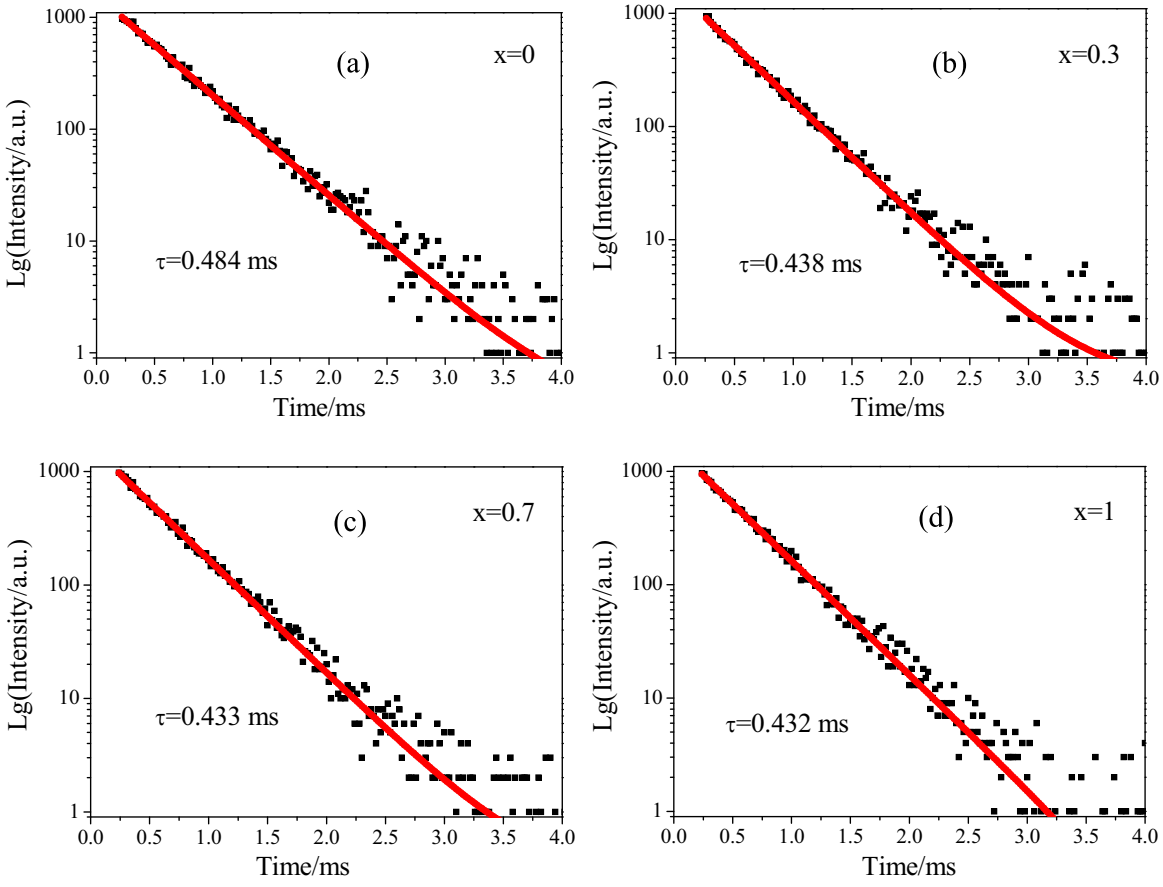

Fig. 8. Luminescence decay curves (λ_{ex}=465 nm) of $Na_{1-x}Li_xLa_{0.95}Eu_{0.05}MgWO_6$ (a: x=0; b: x=0.3; c: x=0.7; d: x=1).

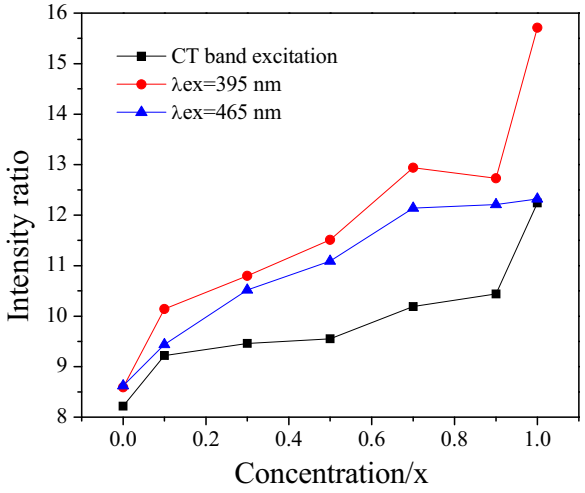

Fig. 9. Emission intensity ratio of $^5D_0$-$^7F_2$/$^5D0$-$^7F_1$ transition for $Na_{1-x}Li_xLa_{0.95}Eu_{0.05}MgWO_6$ phosphors (x=0, 0.1, 0.3, 0.5, 0.7, 0.9, 1) under different excitations.

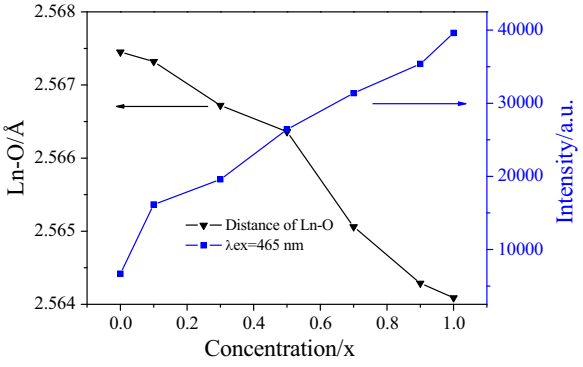

Fig. 10. Relationship between the intensity of $^5D_0$-$^7F_2$ (λ_{ex}=465 nm) and Ln-O bond distance of $Na_{1-x}Li_xLa_{0.95}Eu_{0.05}MgWO_6$ (x=0, 0.1, 0.3, 0.5, 0.7, 0.9, 1).

intra-4f transitions of Eu^{3+}, which were at 395 nm ($^7F_0$-$^5L_6$ transitions) and 465 nm ($^7F_0$-$^5D_2$ transitions) for all compositions. The presence of a CTB in the excitation spectrum when monitored for Eu^{3+} emissions (615 nm) was a clear indication of the non-radiative energy transfer from the host to Eu^{3+}. Upon increasing the Li^+ concentration, the absorption intensity of CTB varied in a small range, whereas the absorption intensities of the 4f−4f transitions of Eu^{3+} monotonically increased. Accordingly, the electric dipole transition intensities of the $Na_{1-x}Li_xLa_{0.95}Eu_{0.05}MgWO_6$ phosphors also monotonically increased under the excitations of 395 nm and 465 nm (Fig. 7), and they reached the maximum for a complete substitution. The luminescence intensities of the $^5D_0$-$^7F_2$ transition for x=1 were enhanced by approximately ten and six times comparing to that of x=0 under the excitations of 395 nm and 465 nm, respectively. In contrast, upon increasing the Li^+ concentration, the electric dipole transition intensities varied in a small range under the excitation of the charge transfer band. The emission intensity of λ_{ex}=395 nm surpassed the intensity of the charge transfer band excitation at $x>0.7$, while the intensity of λ_{ex}=465 nm surpassed the intensity of the charge transfer band excitation at $x\geq 0.5$. It was also significant that the emission intensities of λ_{ex}=465 nm were stronger than those of λ_{ex}=395 nm for all compositions.

The decay curves (λ_{ex}=465 nm) of $Na_{1-x}Li_xLa_{0.95}Eu_{0.05}MgWO_6$

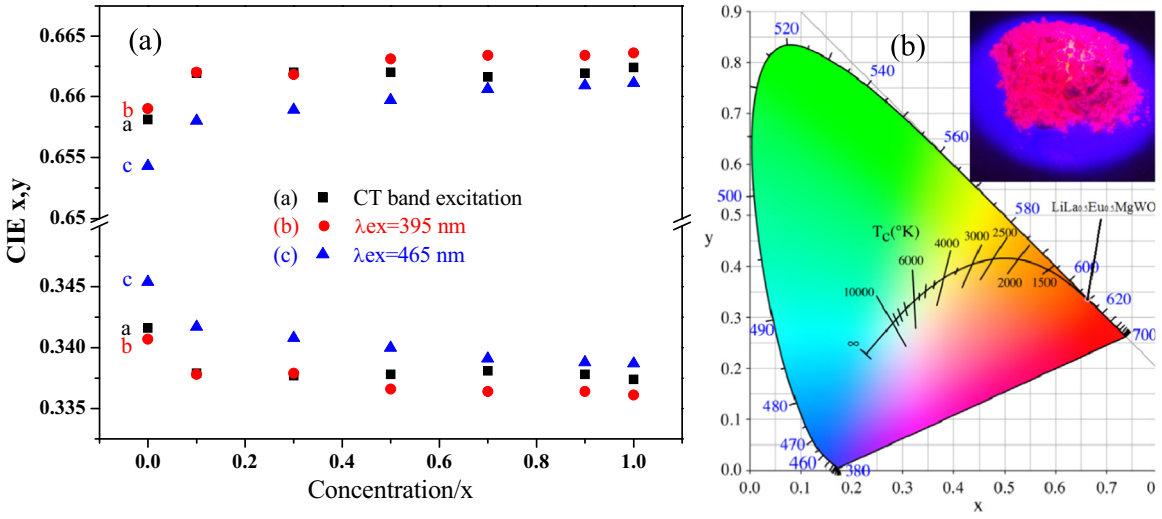

Fig. 11. (a) CIE chromaticity coordinates of $Na_{1-x}Li_xLa_{0.95}Eu_{0.05}MgWO_6$ (x=0, 0.1, 0.3, 0.5, 0.7, 0.9, 1) under different excitations and (b) the photo of $LiLa_{0.5}Eu_{0.5}MgWO_6$ phosphor.)

(x=0, 0.3, 0.7, 1) phosphors are shown in Fig. 8. All of the data are fitted with a single experimental function $I=I_0\exp(-t/\tau)$, where I_0 is the initial emission intensity for t=0, and τ is the decay lifetime. The calculated lifetimes are summarized in Fig. 8. It is clear that the $^5D_0$ lifetime of Eu^{3+}-doped $Na_{1-x}Li_xLaMgWO_6$ decreased upon increasing the concentration x. Usually, for a given emitting ion, a long decay time was characteristic of the most symmetrical surroundings, while a short decay value was observed when site distortion occurred [29]. Increasing the Li^+ ion concentration led to decreased tolerance factors and lower symmetry and thereby a shorter $^5D_0$ lifetime.

According to the Judd-Ofelt theory, the magnetic dipole transition is permitted. However, the electric dipole transition is allowed only when the europium ion occupies a site without an inversion center, and the intensity is significantly affected by the symmetry in the local environments around the Eu^{3+} ions [29]. If the Eu^{3+} ions occupy an inversion symmetry site, the magnetic dipole transition $^5D_0$-$^7F_1$ is dominant. On the other hand, for the electronic dipole transition, $^5D_0$-$^7F_2$ is the dominant transition. The intensity ratio of R=I ($^5D_0$-$^7F_2$)/I ($^5D_0$-$^7F_1$) is a measure of the Eu^{3+} ion's site symmetry, and the emission intensity ratio of $^5D_0$-$^7F_2$ (615 nm)/$^5D_0$-$^7F_1$ (590 nm) for $Na_{1-x}Li_xLa_{0.95}Eu_{0.05}MgWO_6$ phosphors under different excitations is shown in Fig. 9. The ratios tended to increase and varied in a broad range for all three excitations upon increasing the Li^+ concentration. The ratio increased from 8.59 to 15.71 under the excitation of 395 nm, which means that the electric dipole transition held a dominant position. Upon increasing the concentration of Li^+, the tolerance factor gradually decreased, and the structure deviated from the ideal cubic phase, leading to a lower symmetry of the structure. For the hypersensitive electronic dipole transition, the parity-forbidden transition was broken because of the gradually decreased symmetry. The ratio of the $^5D_0$-$^7F_2$/$^5D_0$-$^7F_1$ transitions increased upon increasing the concentration of Li^+, and then the red emission played a dominant role.

As we said above, the decreased tolerance factor and the high distortion coordination polyhedron around Eu^{3+} would further break the parity forbiddenness, so the transition probability of the electric dipole transition would increase. At the same time, in the structure of Eu^{3+}-O^{2-}-A^+, when A^+=Li^+, the covalence between the activator Eu^{3+} and the anion (O^{2-}) would increase due to the smaller ionic radius (0.92 Å < 1.39 Å(Na^+)). This would further enhance the luminescence of the electric dipole transition of Eu^{3+}. In addition, when Li^+ substitutes for Na^+, the lattice volume gradually decreased (Table 1), and the mean bond length of Ln-O also decreased (data according to the structure refinement). The change in the bond length of Ln-O with the luminescence intensity is shown in Fig. 10, with a short bond length corresponding to a higher luminescence intensity. A short bond length means a strong crystal field, which is beneficial to the energy transfer and thus enhances the luminescence of Eu^{3+}. The greatly enhanced radiation transition of the electric dipole of Eu^{3+} and shortened lifetime were due to the low crystal symmetry and especially the shortened Eu-O bond length. This is called "A site inducing energy transfer" [20], which results in a luminescence enhancement of Eu^{3+} in double perovskite. Here, the "A site inducing energy transfer" was proven to be effective. This regularity will continue guiding us to further choose other host elements to enhance the luminescence of Eu^{3+} and will provide guidance for the performance enhancement in other rare earth ion doped luminescence materials.

Fig. 11 shows the CIE chromaticity coordinates of $Na_{1-x}Li_xLa_{0.95}Eu_{0.05}MgWO_6$ phosphors under different excitations and a photo of a $LiLa_{0.5}Eu_{0.5}MgWO_6$ phosphor. The coordinates gradually approach those of standard red light (0.67, 0.33), with an increased R/O value. The coordinates of $LiLa_{0.95}Eu_{0.05}MgWO_6$ under the excitation of 395 nm were (0.6636, 0.3361), which are rather close to the edge of the CIE diagram. This means that the substitution of Li^+ to Na^+ not only enhances the luminescence intensity and availability of different excitation chips but also greatly optimizes the red light quality.

4. Conclusions

In this paper, a series of $Na_{1-x}Li_xLa_{0.95}Eu_{0.05}MgWO_6$ phosphors were successfully synthesized. The ODS/CS for both the A-sites and B-sites reached maximum values at x=0.5. The weakened Raman $T_{2g}(1)$ mode resulted from A-site doping, while the weakened A_{1g} mode resulted from the SOJT distortion of the B' cations. The enhanced luminescence intensity under the excitation of near-UV light or blue light was achieved by selecting a substitution element with a smaller radius by substituting Na^+ with Li^+. The decreased lifetime, increased intensity ratio of red/orange emission and optimized red light quality resulted from the decreased symmetry. The "A site inducing energy transfer" was proven to be effective, and this regularity would continue to guide us to choose other

host elements to enhance the luminescence of Eu^{3+}.

Acknowledgments

The author acknowledges the generous financial support from the Priority Academic Program Development of Jiangsu Higher Education Institutions (PAPD) and the National Natural Science Foundation of China (51402133, 51202111).

References

[1] S. Sekar, P. Arunkumar, D. Jeyakumar, N. Lakshminarasimhan, White light emission in alkali metal ion co-doped single host lattice phosphor $Sr_3B_2O_6$: Ce^{3+},Eu^{2+},A+[A=Li, Na and K], Ceram. Int. 41 (3) (2015) 3497–3501.
[2] L. Tian, L. Wang, L. Zhang, Q. Zhang, W. Ding, M. Yu, Enhanced luminescence of Dy^{3+}/Bi^{3+} co-doped $Gd_3Al_5O_{12}$ phosphors by high-efficiency energy transfer, J. Mater. Sci. Mater. Electron. 26 (2015) 8507–8514.
[3] P. Pust, V. Weiler, C. Hecht, A. Tucks, A.S. Wochnik, A.K. Henss, D. Wiechert, C. Scheu, P.J. Schmidt, W. Schnick, Narrow-band red-emitting Sr[LiAl(3)N(4)]: Eu(2)(+) as a next-generation LED-phosphor material, Nat. Mater. 13 (9) (2014) 891–896.
[4] R. Cao, Q. Xiong, W. Luo, D. Wu, X. Fen, X. Yu, Synthesis and luminescence properties of efficient red phosphors $SrAl_4O_7$:Mn^{4+},R+(R+=Li+, Na+, and K+) for white LEDs, Ceram. Int. 41 (5) (2015) 7191–7196.
[5] R. Yu, R. Luan, C. Wang, J. Chen, Z. Wang, B.K. Moon, J.H. Jeong, Photoluminescence properties of green-emitting $ZnGa_2S_4$:Eu^{2+} phosphor, J. Electrochem. Soc. 159 (5) (2012) J188–J192.
[6] H. Ju, X. Deng, Z. Weng, Q. Wu, B. Wang, Y. Ma, H. Wang, $LiSr_3SiO_4Cl_3$-a novel host lattice for Eu^{2+}-activated luminescent materials, Ceram. Int. 42 (6) (2016) 6846–6849.
[7] F. Liu, Y. Fang, J. Hou, N. Zhang, Z. Ma, Garnet-based red emitting phosphors $Li_6MLa_2Nb_2O_{12}$: Eu^{3+}(M=Ca, Sr, Ba): photoluminescence improvement by changing crystal lattice, Ceram. Int. 40 (2) (2014) 3237–3241.
[8] V. Sivakumar, U.V. Varadaraju, Synthesis, phase transition and photoluminescence studies on Eu^{3+}-substituted double perovskites—a novel orange-red phosphor for solid-state lighting, J. Solid State Chem. 181 (12) (2008) 3344–3351.
[9] Y.P. Liu, H.R. Fuh, Y.K. Wang, Expansion research on half-metallic materials in double perovskites of $Sr_2BB'O_6$ (B=Co, Cu, and Ni; B′=Mo, W, Tc, and Re; and BB′=FeTc), Comput. Mater. Sci. 92 (2014) 63–68.
[10] Y. Huang, H.J. Seo, The Spectroscopy and micro-structure of Eu^{3+} ions doped double perovskite $Ba_3Y_2WO_9$, J. Electrochem Soc. 158 (7) (2011) J215–J220.
[11] S.K. Gupta, M. Sahu, P.S. Ghosh, D. Tyagi, M.K. Saxena, R.M. Kadam, Energy transfer dynamics and luminescence properties of Eu(3+) in $CaMoO_4$ and $SrMoO_4$, Dalton Trans. 44 (43) (2015) 18957–18969.
[12] F. Cheng, Z. Xia, M.S. Molokeev, X. Jing, Effects of composition modulation on the luminescence properties of Eu(3+) doped $Li_{1-x}Ag_xLu(MoO_4)_2$ solid-solution phosphors, Dalton Trans. 44 (41) (2015) 18078–18089.
[13] H. Sun, Q. Zhang, X. Wang, C. Bulin, R.J. Xie, Strong red emissions in Pr^{3+}-doped $(K_{0.5}Na_{0.5})NbO_3$-$CaTiO_3$ diphase ceramics, J. Am. Ceram. Soc. 98 (2) (2015) 601–606.
[14] L. Zhang, B. Sun, Q. Liu, N. Ding, H. Yang, L. Wang, Q. Zhang, Novel layered perovskite $Sr_3Ti_2O_7$:Eu^{3+} phosphor with high-efficiency luminescence enhanced by charge compensation, J. Alloy. Compd. 657 (2016) 27–31.
[15] Z. Fen, T. Wanjun, J. Ballato, Tunable color of Eu^{2+}/Mn^{2+} coactivated $Na_5Ca_2Al(PO_4)_4$ via energy transfer, J. Am. Ceram. Soc. 97 (10) (2014) 3252–3256.
[16] H. Yu, D. Deng, L. Chen, D. Chen, J. Zhong, H. Zhao, S. Xu, Luminescent properties of novel $Ca_{2.89}Mg_{0.11}(PO_4)_2$:$Eu^{2+}$ single-phase white light-emitting phosphor for white LEDs, Ceram. Int. 41 (3) (2015) 3800–3805.
[17] S. Ye, C.H. Wang, Z.S. Liu, J. Lu, X.P. Jing, Photoluminescence and energy transfer of phosphor series $Ba_{2-z}Sr_zCaMo_{1-y}WyO_6$:Eu,Li for white light UVLED applications, Appl. Phys. B 91 (3–4) (2008) 551–557.
[18] L. Zhang, P. Han, Y. Han, Z. Lu, H. Yang, L. Wang, Q. Zhang, Structure evolution and tunable luminescence of $(Sr_{0.98-m}BamEu_{0.02})2Ca(Mo_{1-n}Wn)O_6$ phosphor with ultraviolet excitation for white LEDs, J. Alloy. Compd. 558 (2013) 229–235.
[19] Z. Xia, J. Sun, H. Du, D. Chen, J. Sun, Luminescence properties of double-perovskite Sr_2Ca_{1-2x} $Eu_xNa_xMoO_6$ red-emitting phosphors prepared by the citric acid-assisted sol–gel method, J. Mater. Sci. 45 (6) (2009) 1553–1559.
[20] L. Zhang, Q. Liu, N. Ding, H. Yang, J. Zhang, Q. Zhang, Enhanced Luminescence of Double Perovskite Na(La,Gd)$MgWO_6$: Eu^{3+} phosphor based on A-site-induced energy transfer, Sci. Adv. Mater. doi: 10.1166/sam.2015.2318.
[21] L. Zhang, Q. Liu, N. Ding, H. Yang, L. Wang, Q. Zhang, Dual-channel enhanced luminescence of double perovskite $NaGdMgWO_6$:Eu^{3+} phosphor based on alternative excitation and delayed quenching, J. Alloy. Compd. 642 (2015) 45–52.
[22] J. Hou, X. Yin, F. Huang, W. Jiang, Synthesis and photoluminescence properties of $NaLaMgWO_6$:RE^{3+}(RE=Eu, Sm, Tb) phosphor for white LED application, Mater. Res. Bull. 47 (6) (2012) 1295–1300.
[23] X. Yin, Y. Wang, F. Huang, Y. Xia, D. Wan, J. Yao, Excellent red phosphors of double perovskite Ca_2LaMO_6:Eu (M=Sb, Nb, Ta) with distorted coordination environment, J. Solid State Chem. 184 (12) (2011) 3324–3328.
[24] M.C. Knapp, P.M. Woodward, A-site cation ordering in AA′BB′O6 perovskites, J. Solid State Chem. 179 (4) (2006) 1076–1085.
[25] G. King, L.M. Wayman, P.M. Woodward, Magnetic and structural properties of $NaLnMnWO_6$ and $NaLnMgWO_6$ perovskites, J. Solid State Chem. 182 (6) (2009) 1319–1325.
[26] L. Zhang, Z. Lu, P. Han, L. Wang, Q. Zhang, Synthesis and photoluminescence of Eu^{3+}-activated double perovskite NaGdMg(W, Mo)O^{6-} a potential red phosphor for solid state lighting, J. Mater. Chem. C 1 (1) (2013) 54–57.
[27] G. King, S. Thimmaiah, A. Dwivedi, P.M. Woodward, Synthesis and characterization of new AA′BWO6 perovskites exhibiting simultaneous ordering of A-site and B-site cations, Chem. Mater. 19 (2007) 6451–6458.
[28] S. Ye, C.-H. Wang, X.-P. Jing, Photoluminescence and Raman spectra of double-perovskite Sr[sub 2]Ca(Mo/W)O[sub 6] with A- and B-site substitutions of Eu^{3+}, J. Electrochem Soc. 155 (6) (2008) J148–J151.
[29] R. Yu, C. Wang, J. Chen, Y. Wu, H. Li, H. Ma, Photoluminescence characteristics of Eu^{3+}-doped double-perovskite phosphors, ECS J. Solid State Sci. 3 (3) (2014) R33–R37.